Optical Hyperlens: Far-field imaging beyond the diffraction limit

Zubin Jacob, Leonid V. Alekseyev and Evgenii Narimanov

Department of Electrical Engineering, Princeton University
Princeton, New Jersey - 08540
evgenii@princeton.edu

Abstract: We propose an approach to far-field optical imaging beyond the diffraction limit. The proposed system allows image magnification, is robust with respect to material losses and can be fabricated by adapting existing metamaterial technologies in a cylindrical geometry.

OCIS codes: (110.0180) Microscopy; (160.1190) Anisotropic optical materials

References and links

1. B. Hecht, B. Sick, U. P. Wild, V. Deckert, R. Zenobi, O. J. F. Martin and D. W. Pohl, "Scanning near-field optical microscopy with aperture probes: Fundamentals and applications," J. Chem. Phys. **112**, 7761 (2000).
2. J. B. Pendry, "Negative refraction makes a perfect lens," Phys. Rev. Lett. **85**, 3966-3969 (2000).
3. V. G. Veselago, "The electrodynamics of substances with simultaneously negative values of permittivity and permeability," Sov. Phys. Usp. **10**, 509 (1968).
4. R. A. Shelby, D. R. Smith, and S. Schultz,"Experimental verification of a negative index of refraction," Science **292**, 77-79 (2001).
5. V. M. Shalaev, W. Cai, U. K. Chettiar, H.-K. Yuan, A. K. Sarychev, V. P. Drachev, and A. V. Kildishev, "Negative index of refraction in optical metamaterials," Opt. Lett. **30**, 3356-3358 (2005), http://www.opticsinfobase.org/abstract.cfm?URI=ol-30-24-3356.
6. V. A. Podolskiy and E. E. Narimanov, "Near-sighted superlens," Opt. Lett. **30**, 75-77 (2005), http://www.opticsinfobase.org/abstract.cfm?URI=ol-30-1-75.
7. R. Merlin, "Analytical solution of the almost-perfect-lens problem," Appl. Phys. Lett. **84**, 1290-1292 (2004).
8. K. J. Webb, M. Yang, D. W. Ward, and K. A. Nelson, "Metrics for negative-refractive-index material," Phys. Rev. E **70**, 035602(R) (2004).
9. C. Luo, S. G. Johnson, J. D. Joannopoulos, and J. B. Pendry, "All-angle negative refraction without negative effective index," Phys. Rev. B **65**, 201104-1-201104-4 (2002).
10. V. A. Podolskiy, and E. E. Narimanov, "Strongly anisotropic waveguide as a nonmagnetic left-handed system," Phys. Rev. B **71**, 201101 (2005).
11. V. A. Podolskiy, L. Alekseyev, and E. E. Narimanov, "Strongly anisotropic media: the THz perspectives of left-handed materials", J. Mod. Opt. **52**(16) 2343 (2005).
12. R. Wangberg, J. Elser, E. E. Narimanov, and V. A. Podolskiy, "Non-magnetic nano-composites for optical and infrared negative refraction index media," J. Opt. Soc. Am. B. **23**, 498 (2006).
13. A. A. Govyadinov and V. A. Podolskiy, "Meta-material photonic funnels for sub-diffraction light compression and propagation," Phys. Rev. B **73**(15), 155108 (2006).
14. D. R. Smith and D. Schurig, " Electromagnetic Wave Propagation in Media with Indefinite Permittivity and Permeability Tensors,"Phys. Rev. Lett. **90**, 077405 (2003).
15. T. C. T. Ting, "New solutions to pressuring, shearing, torsion, and extension of a cylindrically anisotropic elastic circular tube or bar," Proc. Roy. Soc. London, A455, 3527-3542 (1999).
16. N. Fang, H. Lee, C. Sun and X. Zhang, "Sub-diffraction-limited optical imaging with a sliver superlens," Science **308**, 534-537 (2005).

1. Introduction

Resolution of conventional optics is generally constrained by the diffraction limit, which prevents imaging of subwavelength features. Such fine details are encoded in rapid spatial varia-

#72534 - $15.00 USD Received 30 June 2006; accepted 4 August 2006

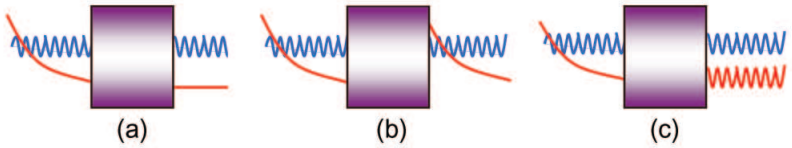

Fig. 1. (a) A conventional imaging system transforms propagating waves, but does not operate on the decaying evanescent waves; these waves can only be detected in the near field. (b) "Superlens" amplifies the evanescent waves but does not change their decaying character. (c) An ideal device would convert evanescent waves to propagating waves for ease of detection and processing; these waves should not mix with the propagating waves emanating from the object.

tions of electromagnetic fields at the object's surface. However, these fields decay exponentially with distance and are thus only detectable in the near field [Fig. 1(a)]. Outside the near field, the loss of high spatial frequency information carried by the decaying evanescent waves precludes reconstructing the image of an object with resolution better than $\lambda/2$.

Subwavelength optical imaging in the near field can be performed via near field scanning optical microscopy, whereby the exponentially decaying evanescent waves are detected by a scanning probe [1]. While successful in resolving subwavelength structures, this serial technique suffers from several drawbacks, including low throughput, the necessity for substantial post-processing of the scanning probe data, and inability to simultaneously observe different parts of the imaged object. It is highly desirable for many applications (e.g. biological microscopy) to use a system which would produce a direct optical far field image that includes subwavelength features. It is for this reason that the recently proposed "superlens" [2] – a device capable of subwavelength resolution that relies on materials with negative index of refraction [3, 4, 5] received much attention.

The originally proposed superlens would not only focus the propagating waves, but would also amplify the evanescent waves in such a way that both the propagating and evanescent fields would contribute to an image in the far field, resulting in resolution far below the diffraction limit [Fig. 1(b)]. However, subsequent studies demonstrated that due to the resonant nature of the enhancement of evanescent waves the subwavelength resolving power of most superlens implementations is severely curtailed by material losses [6, 7, 8] or the characteristic patterning of the negative index systems [9]. Furthermore, although a superlens amplifies evanescent modes and thus in principle enables their detection, the evanescent waves cannot be processed or brought to focus by conventional optics.

An ideal imaging device would avoid this problem: it would not only capture evanescent fields to retrieve subwavelength information, but would also allow for their processing with standard optical components. This could be accomplished by transferring the information carried by evanescent fields into a portion of the propagating spectrum [Fig. 1(c)]. Following the conversion, these propagating waves would be detected and processed in the far field by methods similar to those of conventional imaging.

Here we propose a device capable of forming a magnified optical image of a subwavelength object in the far field. This device relies on recently proposed strongly anisotropic metamaterials that feature opposite signs of the two permittivity tensor components, $\varepsilon_{\parallel}$ and $\varepsilon_{\perp}$ [10, 11, 12]. Such metamaterials have been theoretically shown to support propagating waves with very large wavenumbers [10, 13] (in ordinary dielectrics, such high-k modes undergo evanescent decay). This unusual property arises from the *hyperbolic* functional form of the dispersion relation for such metamaterials, and is the key feature enabling subwavelength resolution of our proposed device. It is for this reason that we call our imaging device *the hyperlens*.

#72534 - $15.00 USD Received 30 June 2006; accepted 4 August 2006

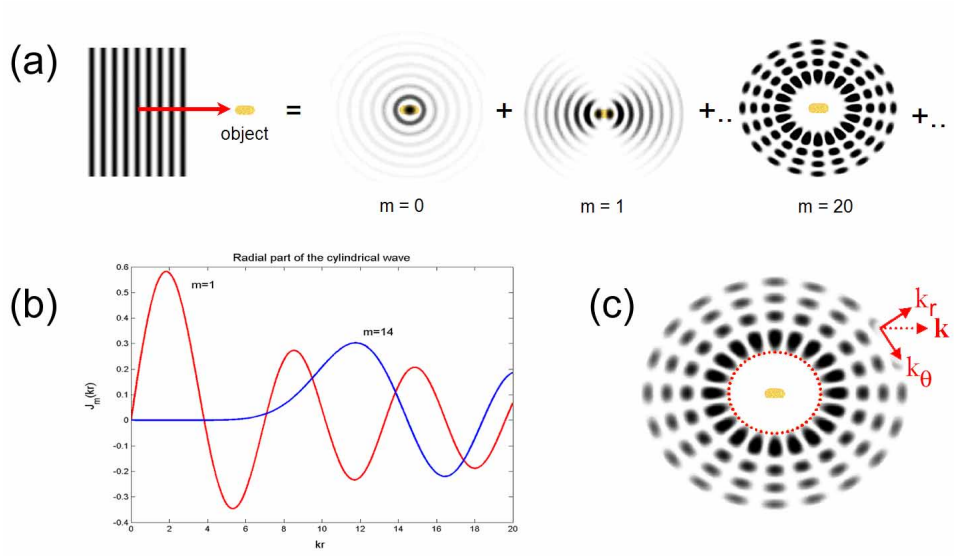

Fig. 2. (a) Scattering of an incident plane wave by a target (yellow object) can be represented as scattering of various angular momentum modes (the regions of high intensity are shown in black and low intensity in white). Higher order modes are exponentially small at the center (b). This results from an upper bound on values of k_θ and the formation of the caustic shown in red in (c).

The hyperlens utilizes cylindrical geometry to magnify the subwavelength features of imaged objects so that these features are above the diffraction limit at the hyperlens output. Thus, the output of the hyperlens consists entirely of propagating waves, which can be processed by conventional optics. Furthermore, our simulations show that material losses do not appreciably degrade the performance of the proposed device due to its non-resonant nature.

2. Angular Momentum States as Information Channels

Conventional lenses image objects by applying an appropriate phase transformation to the propagating waves, bringing them to focus at a certain distance beyond the lens. However, a conventional lens does not operate on the evanescent waves emanating from the object. As such, the evanescent fields are lost. This apparent loss of information restricts a regular lens from reconstructing the image of an object with a resolution better than $\lambda/2$. Converting the evanescent waves to propagating waves without mixing is the key to extracting the subwavelength information in the far field.

In traditional discussions of imaging, waves scattered by the object are examined in a monochromatic plane wave basis with a wide spectrum of spatial frequencies. The choice of basis, however, is dictated by the symmetry of the object under consideration and/or by convenience. Mathematically, the problem can be equivalently treated in a basis of cylindrical waves. In particular, any plane wave illuminating an object can be expanded in a basis of cylindrical waves as

$$\exp(ikx) = \sum_{m=-\infty}^{m=\infty} i^m J_m(kr)\exp(im\phi), \tag{1}$$

where $J_m(kr)$ denotes the Bessel function of the first kind and m is the angular momentum mode number of the cylindrical wave [this decomposition is illustrated schematically in Fig. 2(a)]. In

#72534 - $15.00 USD Received 30 June 2006; accepted 4 August 2006

this representation, reconstructing an image is equivalent to retrieving the scattering amplitudes and phase shifts of the various constituent angular momentum modes. The resolution limit in the cylindrical wave basis can be restated as the limit to the number of retrieved angular momentum modes with appreciable amplitude or phase change after scattering from the object.

We may think of the scattered angular momentum modes as distinct information channels through which the information about the object at the origin is conveyed to the far field. However, even though the number of these channels is infinite [m is unbounded in expansion (1)], very little information is carried over the high-m channels. As evidenced by Fig. 2(b), which shows the exact radial profile of the electric field for m=1 and m=14, for high values of m the field exponentially decays at the origin. This suggests that the interaction between a high-m mode and an object placed at the origin is exponentially small, i.e. the scattering of such modes from the object is negligible. Classically, this corresponds to the parts of an illuminating beam that have a high 'impact parameter' and therefore miss the scatterer.

Exponential decay of high-m modes at the center can also be seen as a result of conservation of angular momentum,

$$m = k_\theta r, \tag{2}$$

where m is the angular momentum mode number, k_θ is the tangential component of the wave vector and r is the distance from the center. Conservation law (2) implies that the tangential component of the wave vector increases towards the center, i.e. $k_\theta \propto 1/r$. On the other hand, the dispersion relation in an isotropic medium such as vacuum constrains the allowed radial and tangential components of the wave vector to lie on a circle [Fig. 3(a)]:

$$k_r^2 + k_\theta^2 = \varepsilon \frac{\omega^2}{c^2}. \tag{3}$$

Thus, as the tangential component of the wave vector increases towards the center there comes a point when the radial component of the wave vector vanishes. This classical turning point – the boundary at which the incoming wave turns back – corresponds to the caustic [Fig. 2(c)]. Inside the caustic, the angular momentum states become evanescent. Using $m = k_\theta r$ in the dispersion relation (3) to find when $k_r = 0$ yields the radius of the caustic, $R_c \propto m\lambda$. Thus, the caustic radius increases with angular momentum and the circumference of the caustic corresponds exactly to m wavelengths – i.e. the distance between each of the m nodes in an angular momentum mode m is λ at a distance R_c from the center.

3. Angular Momentum States in Strongly Anisotropic Media and the Hyperlens

The existence of the caustic, and hence the exponential decay of the field for $r < R_c$, is a consequence of the upper bound on k_θ dictated by the functional form of dispersion relation (3). This functional form, however, becomes different for anisotropic materials due to the dependence of dielectric response on wave propagation direction.

In the case of uniaxial anisotropy, dielectric permittivity is characterized by two values: $\varepsilon_\parallel$ along the optical axis of the crystal, and $\varepsilon_\perp$ transverse to the optical axis. Propagating modes, in turn, can be decomposed into two polarization states: the *ordinary* (TE) and *extraordinary* (TM) waves. For ordinary (TE) waves, the electric field vector is transverse to the optical axis and produces the same dielectric response (given by $\varepsilon_\perp$) independent of wave propagation direction. However, for the extraordinary (TM) waves, the electric field vector has components both along and transverse to the optical axis. Accordingly, both $\varepsilon_\parallel$ and $\varepsilon_\perp$ play a role in the dielectric response and in the dispersion relation, given by

$$\frac{k_\perp^2}{\varepsilon_\parallel} + \frac{k_\parallel^2}{\varepsilon_\perp} = \frac{\omega^2}{c^2}, \tag{4}$$

#72534 - $15.00 USD Received 30 June 2006; accepted 4 August 2006

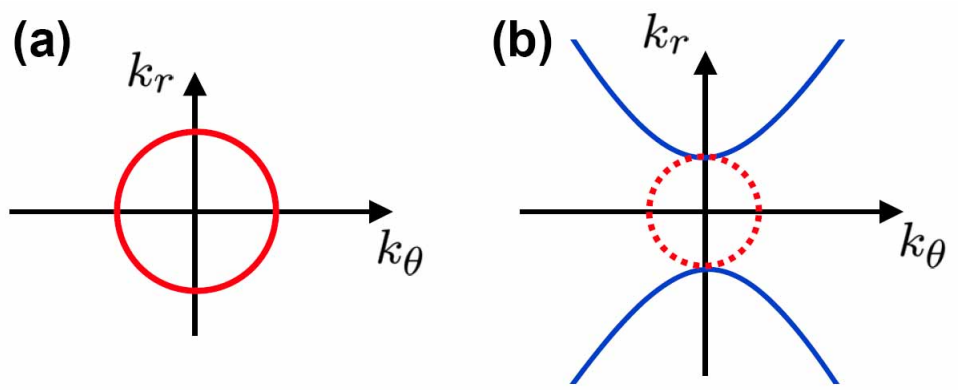

Fig. 3. Dispersion relation for isotropic medium (a) and for a material with $\varepsilon_r < 0$, $\varepsilon_\theta > 0$ (b). Note that for a fixed frequency, the wave vector k can take on arbitrarily large values (within the effective medium approximation).

where $k_\perp$ and $k_\parallel$ refer to wave vector components normal or parallel to the optical axis. Evidently, the allowed k values for the TM waves describe an ellipse.

In the case of strong anisotropy where $\varepsilon_\perp$ and $\varepsilon_\parallel$ are of opposite signs, the dispersion relation (4) becomes *hyperbolic* [Fig. 3(b)]. Materials with such anisotropy (sometimes referred to as indefinite media [14]) enable photonic structures with unusual features, including adiabatic wavelength compression and highly confined guided modes with very large cutoff [10, 13]. These phenomena arise due to unbounded values of wave vector k at a finite frequency, allowed by the hyperbolic dispersion relation.

We consider now extraordinary waves (TM modes) in a bulk medium with strong *cylindrical anisotropy* where dielectric permittivities have different signs in the tangential and radial directions ($\varepsilon_\theta > 0$, $\varepsilon_r < 0$). The hyperbolic dispersion relation

$$\frac{k_r^2}{\varepsilon_\theta} - \frac{k_\theta^2}{|\varepsilon_r|} = \frac{\omega^2}{c^2} \tag{5}$$

allows for very high values of k, limited only by the material scale of the medium. As the tangential component of the wave vector increases towards the center, the radial component also increases; Eq. 5 can be satisfied for any radius and any value of m. Thus, as long as the effective medium description is valid, there is no caustic, and the field of high angular momentum states has appreciable magnitude close to the center.

The cylindrical TM mode solution for the ($\varepsilon_\theta > 0$, $\varepsilon_r < 0$) anisotropy above is given by

$$B_z \propto J_{m\sqrt{\varepsilon_r/\varepsilon_\theta}}\left(\frac{\omega}{c}\sqrt{\varepsilon_\theta}\right)\exp(im\phi). \tag{6}$$

This mode is plotted in Fig. 4(b). Note that the cylindrical anisotropy causes a high angular momentum state to penetrate toward the center – in contrast to the behavior of high-m modes in regular dielectrics [see Fig. 4(a)].

We now consider a hollow core cylinder of inner radius $R_{\text{inner}} \sim \lambda$ and outer radius R_{outer}, made of a cylindrically anisotropic homogeneous medium. The high angular momentum states with radius of the caustic $R_c \leq R_{\text{outer}}$ are captured by the device and guided towards the core. In this case, cylindrical symmetry implies that the distance between the field nodes at the core is less than the vacuum wavelength (see Fig. 4). Therefore, such high angular momentum states can act as a subwavelength probe for an object placed inside the core. Furthermore, since in

#72534 - $15.00 USD Received 30 June 2006; accepted 4 August 2006

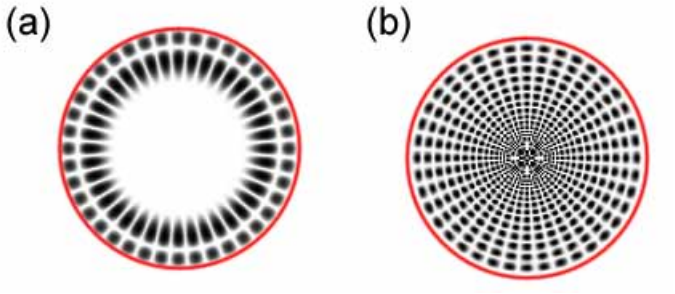

Fig. 4. (a) High angular momentum states in an isotropic dielectric cylinder (b) High angular momentum states in a cylinder made of $\varepsilon_\theta > 0$, $\varepsilon_r < 0$ metamaterial (in the effective medium approximation); note that the field penetrates to the center.

the medium under consideration these states are propagating waves, they can carry information about the detailed structure of the object to the far field. Our proposed device, thus, enables extra information channels for retrieving the object's subwavelength structure. In the absence of the device, the high angular momentum modes representing these channels do not reach the core and as such carry no information about the object.

The resolution of our device (which we refer to as the *hyperlens*) is determined by the effective wavelength at the core and is given by

$$\Delta \propto \frac{R_{\text{inner}}}{R_{\text{outer}}}\lambda. \tag{7}$$

4. Achieving the Cylindrical Anisotropy: Metacylinder Realizations

Cylindrical anisotropy is known in the mechanical properties of tree bark [15], but there exist no natural materials with the desired cylindrical anisotropy in the dielectric response. However, the required anisotropy can be attained using metamaterials, e.g. a hollow core cylinder consisting of 'slices' of metal and dielectric or alternating concentric layers of metal and dielectric (Fig. 5). The layer thickness h in each of these structures is much less than the wavelength λ and when $h \ll \lambda \leq r$ we can treat this finely structured material as an effective medium with

$$\varepsilon_\theta = \frac{\varepsilon_m + \varepsilon_d}{2} \tag{8}$$

$$\varepsilon_r = \frac{2\varepsilon_m \varepsilon_d}{\varepsilon_m + \varepsilon_d}, \tag{9}$$

where ε_m and ε_d denote the dielectric permittivities of the metal and dielectric layers respectively. A low loss cylindrically anisotropic material can also be achieved by metallic inclusions in a hollow core dielectric cylinder.

As described in the previous section, the core of the hyperlens has access to high angular momentum states, which are the far-field subwavelength information channels. The effective wavelength near the core is much less than the free space wavelength. Thus, an object placed inside this hollow core near the periphery will form an image just outside the cylinder with resolution better than $\lambda/2$.

It should be noted that the polar dielectric permittivities are ill defined at the center and any practical realization of cylindrical anisotropy, such as metamaterial structures, can only closely approximate the desired dielectric permittivities away from the center (when $r \geq \lambda$).

#72534 - $15.00 USD Received 30 June 2006; accepted 4 August 2006

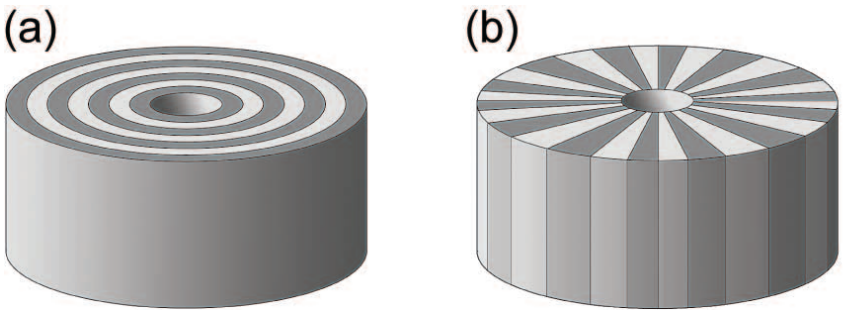

Fig. 5. Possible realizations of metacylinders. Concentric metallic layers alternate with dielectric layers (a) or radially symmetric "slices" alternate in composition between metallic and dielectric (b) to produce ($\varepsilon_\theta > 0$, $\varepsilon_r < 0$) anisotropy. This results in a hyperbolic dispersion relation necessary for penetration of the field close to the center.

Furthermore, the effective medium equations are not valid close to the center and thus singularities exhibited by Eq. 6 as $r \to 0$ are not present in any physical system with $R_{\text{inner}} \sim \lambda$. For $R_{\text{inner}} \geq \lambda$, however, as we shall see in the following section, the effective medium description is adequate.

5. Numerical Simulations

As follows from the preceding discussion, close to the core one cannot rely on the effective medium approximation. Therefore we adopt a numerical approach of solving Maxwell's equations in a hollow core cylinder consisting of alternating layers of metal and dielectric [Fig. 6(a)].

As expected from the theoretical analysis in Section 3, the numerical simulations show that high angular momentum states do indeed penetrate close to the core [Fig. 6(b)]. Also note that this penetrating nature is in sharp contrast to the peripheral behavior of a high angular momentum state with the same mode number in a uniform dielectric hollow core cylinder [Fig. 6(c) and (d)].

To study the imaging characteristics of our device we consider two sources kept inside the core of the hyperlens [Fig. 7(a)], separated by a distance below the diffraction limit. The corresponding intensity pattern is shown in Fig. 7(b) in false color. Note that a conventional optical system cannot resolve such a configuration of sources. The simulation solves for the actual electromagnetic field in each layer taking into account the losses in the metal. The highly directional nature of the beams from two sources placed a distance $\lambda/3$ apart allows for the resolution at the outer surface of the hyperlens. Furthermore, the separation between the two output beams at the boundary of the device is 7 times the distance between the sources and is bigger than the diffraction limit, thereby allowing for subsequent processing by conventional optics. This magnification corresponds to the ratio of the outer and inner radii, and is a consequence of cylindrical symmetry, together with the directional nature of the beams.

To further improve the performance of the proposed system, this hyperlens (which is essentially an evanescent wave to propagating wave converter) can be combined with an evanescent wave enhancer [2, 16] (inner core coating of $\text{Re}[\varepsilon] \approx -1$) to yield higher resolution in the far field. We illustrate this by simulating two sources placed at a distance $\lambda/4.5$ apart ($\lambda = 365$ nm) inside a hyperlens made of 160 alternating layers of silver ($\varepsilon = -2.4012 + 0.2488i$ [16]) and dielectric ($\varepsilon \approx 2.7$), each 10 nm thick. The intensity distribution at the source is shown in Fig. 8(a), whereas the intensity distribution just outside the hyperlens is shown in Fig. 8(b). The two sources are clearly resolved, even though the distance between them is clearly be-

#72534 - $15.00 USD Received 30 June 2006; accepted 4 August 2006

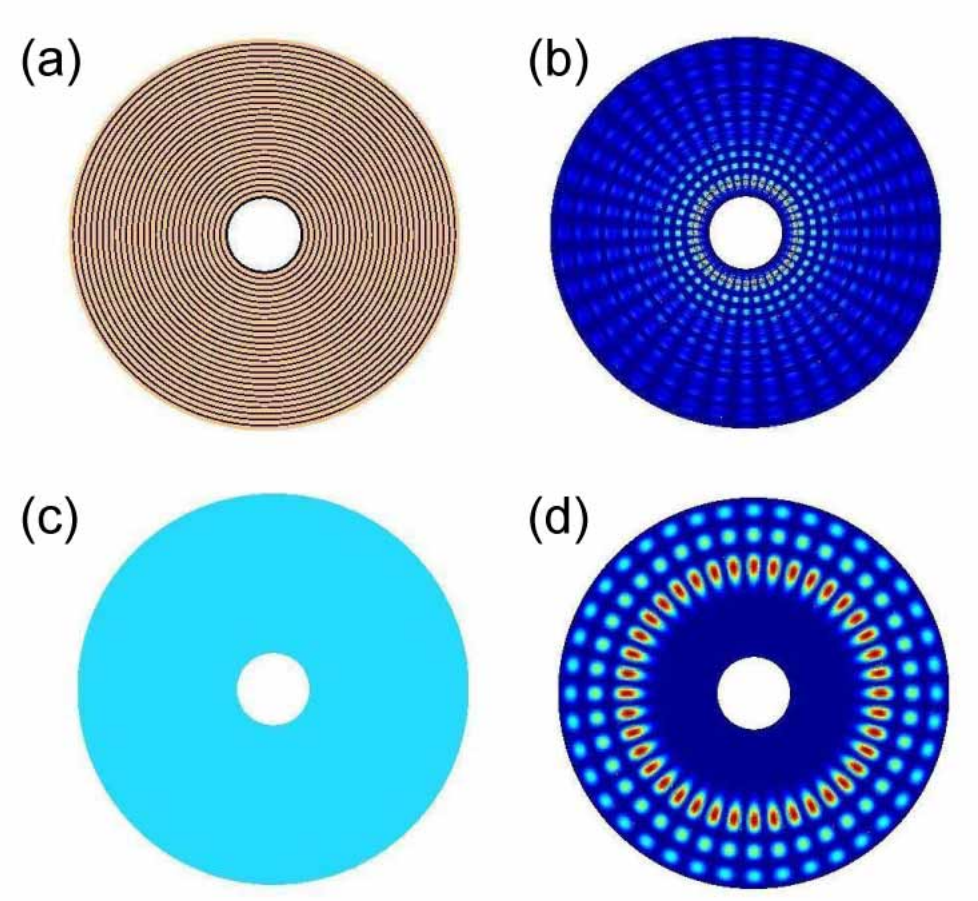

Fig. 6. (a) Top view of the hyperlens made of 50 alternating layers of metal(dark regions) with $\varepsilon_m = -2$ and dielectric (grey regions) with $\varepsilon_d = 5$ .The outer radius is $2.2\mu m$ and the inner radius is $250nm$. (b) Calculated light intensity for m=20 angular momentum state in false color representation where red denotes high intensity and blue corresponds to low intensity. Note the penetrating nature due to the achieved cylindrical anisotropy. (c) A hollow core cylinder of the same geometry made from a uniform dielectric $\varepsilon_{\text{uniform}} = 1.5$ (average of ε_m and ε_d) (d) Corresponding intensity for m=20 mode

#72534 - $15.00 USD Received 30 June 2006; accepted 4 August 2006

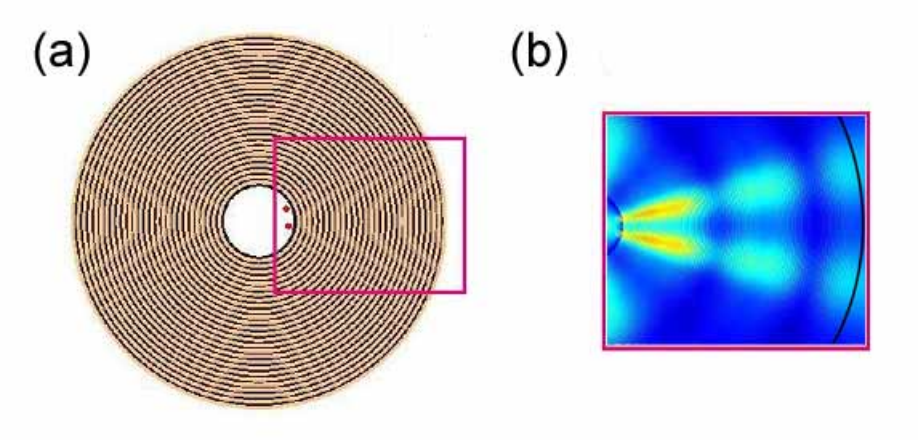

Fig. 7. (a) Schematics of imaging by the hyperlens. Two point sources separated by $\lambda/3$ are placed within the hollow core of the hyperlens consisting of 160 alternating layers of metal ($\varepsilon = -1 + 0.01i$) and dielectric ($\varepsilon = 1.1$) each 10 nm thick (the inner layer of the device is dielectric). The radius of the hollow core is R_{inner}=250 nm, the outer radius R_{outer}=1840 nm, the operating wavelength is 300 nm and the distance between the sources is 100 nm. (b) False color plot of intensity in the region bounded by the rectangle showing the highly directional nature of the beams from the two point sources. The boundary is shown in black where the separation between the beams is much greater than λ due to magnification.

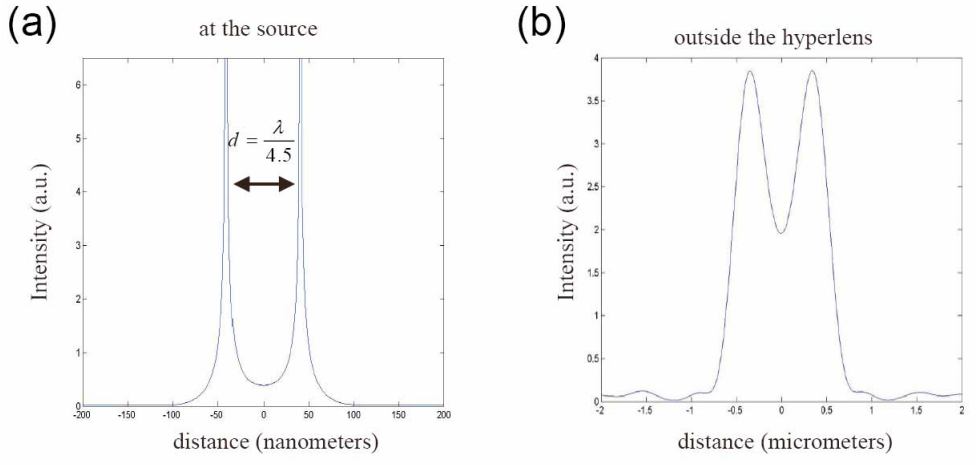

Fig. 8. Demonstration of subwavelength resolution in the composite hyperlens containing two sources placed a distance $\lambda/4.5$ apart inside the core. (a): Field at the source. (b): Field outside the hyperlens.

#72534 - $15.00 USD
Received 30 June 2006; accepted 4 August 2006

low the diffraction limit. It should be noted that realistic losses do not significantly affect the sub-diffraction resolution capabilities of the hyperlens. Furthermore, due to the optical magnification in the hyperlens (by a factor of 5 in the simulation of Fig. 8), even for the subwavelength object, the scale of the image can be substantially larger than the wavelength – thus allowing for further optical processing (e.g. further magnification) of the image by conventional optics.

6. Conclusion

We have demonstrated a system that projects an image onto the far field with resolution beyond the diffraction limit. The proposed hyperlens can be realized by adapting existing planar metamaterial technologies to a cylindrical geometry. Our system is capable of magnification, and since the output consists of propagating waves, the optical image can be further manipulated by conventional optics. Furthermore, due to the non-resonant nature of our device, it is not significantly affected by material losses.

Acknowledgements

This work was partially supported by National Science Foundation grants DMR-0134736 and ECS-0400615, and by Princeton Institute for the Science and Technology of Materials (PRISM). We would like to thank Prof. X. Zhang for helpful discussions.

#72534 - $15.00 USD Received 30 June 2006; accepted 4 August 2006